Title	The Deposition densities of radiocesium and the air dose rates in undisturbed fields around the Fukushima Dai-ichi nuclear power plant; Their temporal changes for five years after the accident
Author(s)	Mikami Satoshi, Tanaka Hiroyuki, Matsuda Hideo, Sato Shoji, Hoshide Yoshifumi, Okuda Naotoshi, Suzuki Takeo, Sakamoto Ryuichi, Ando Masaki, Saito Kimiaki
Citation	Journal of Environmental Radioactivity,210,p.105941_1 - 105941_12
Text Version	Published Journal Article
URL	https://jopss.jaea.go.jp/search/servlet/search?5065489
DOI	https://doi.org/10.1016/j.jenvrad.2019.03.017
Right	

Journal of Environmental Radioactivity 210 (2019) 105941

Contents lists available at ScienceDirect

Journal of Environmental Radioactivity

journal homepage: www.elsevier.com/locate/jenvrad

The deposition densities of radiocesium and the air dose rates in undisturbed fields around the Fukushima Dai-ichi nuclear power plant; their temporal changes for five years after the accident

Satoshi Mikami[a,*], Hiroyuki Tanaka[b], Hideo Matsuda[b,1], Shoji Sato[b], Yoshifumi Hoshide[c,2], Naotoshi Okuda[c], Takeo Suzuki[d], Ryuichi Sakamoto[d], Masaki Andoh[a], Kimiaki Saito[e]

[a] Nuclear Emergency Assistance and Training Center, Japan Atomic Energy Agency, 11601-13 Nishi-jusanbugyo, Hitachinaka-city, Ibaraki, 311-1206, Japan
[b] Radioactive Analysis Division, Japan Chemcal Analysis Center; 295-3, Sanno-cho, Inage, Chiba, Chiba, 263-0002, Japan
[c] Division of Emergency Preparedness Technology, Nuclear Safety Technology Center; 5-1-3-101, Hakusan, Bunkyo, Tokyo, 112-8604, Japan
[d] Institute of Radiation Measurements; 2-4 Shirane, Shirakata, Tokai-mura, Naka, Ibaraki, 319-1106, Japan
[e] Japan Atomic Energy Agency, 178-4-4 Wakashiba, Kashiwa, Chiba, 227-0871, Japan

ARTICLE INFO

Keywords:
Fukushima accident
Deposition density
air dose rate
Portable germanium detector
In-situ measurement
Regional distribution
Temporal change

ABSTRACT

The deposition densities of radiocesium and the air dose rates were repeatedly measured in a large number of undisturbed fields within the 80 km zone that surrounds the Fukushima Dai-ichi Nuclear Power Plant site between 2011 and 2016, and features of their temporal changes were clarified. The average air dose rate excluding background radiation in this zone decreased to about 20% of the initial value during the period from June 2011 to August 2016, which was essentially a result of the radioactive decay of ^{134}Cs with a half-life of 2.06 y. The air dose rate reduction was faster than that expected from the decay of radiocesium by a factor of about two, with most of this reduction being attributed to the penetration of radiocesium into the soil. The average deposition densities of ^{134}Cs and ^{137}Cs in fields that were not decontaminated were found to have decreased nearly according to their expected radioactive decay, which indicated that the movement of radiocesium in the horizontal direction was relatively small. The effect of decontamination was apparently observed in the measurements of air dose rates and deposition densities. Nominally, the average air dose rates in the measurement locations were reduced by about 20% by decontamination and other human activities, of which accurate quantitative analysis is and continue to be a challenge. In this paper, new original data obtained during 2013–2016 were added to the previously reported data collected up to 2012, and it is discussed throughout.

1. Introduction

The Great East Japan Earthquake that struck Japan on March 11, 2011 caused the Fukushima Dai-ichi Nuclear Power Plant (FDNPP) accident. Because of the electricity blackout induced by the tsunami that followed the earthquake, cooling functions at the nuclear power plants were significantly damaged. As a result, a significant amount and many different kinds of radionuclides were released into the atmosphere (NISA, 2011; IAEA, 2015), and deposition of multiple radionuclides, such as ^{134}Cs, ^{137}Cs, ^{131}I, ^{129m}Te, ^{110m}Ag, ^{89}Sr, ^{90}Sr, ^{238}Pu, and $^{239+240}$Pu, has been observed over a widespread area (Saito et al., 2015). The amounts of these radionuclides that were released have been extensively evaluated by many researchers. According to a recent study, the total release of ^{137}Cs was considered to be around 14.5 PBq (Katata et al., 2015), which was less than that from the Chernobyl accident by several factors.

The deposition of released radionuclides on land occurred over wide areas in eastern Japan according to atmospheric dispersions in many different directions. It has since been reported that wet deposition associated with rainfall and snowfall played an important role in this deposition of radionuclides. The area northwest of the FDNPP site was extremely contaminated, and the long-and-narrow-shaped middle part of Fukushima Prefecture also exhibited a relatively high level of contamination. Furthermore, some regions far from the FDNPP site were found to have some degree of contamination.

To obtain basic data to evaluate the impact of the accidental release,

* Corresponding author.
E-mail address: mikami.satoshi@jaea.go.jp (S. Mikami).
[1] Present address: The Secretariat of the Nuclear Regulation Authority, 1-9-9, Roppongi, Minato-ku, Tokyo 106–8450, Japan.
[2] Present address: Advanced Fusion Technology,Co.,Ltd., 5-6-3 Sotokanda, Chiyoda-ku, Tokyo 101–0021, Japan.

https://doi.org/10.1016/j.jenvrad.2019.03.017
Received 30 October 2017; Received in revised form 22 February 2019; Accepted 14 March 2019
Available online 23 March 2019

a national project for comprehensive environmental monitoring was launched in June 2011 (Saito and Onda, 2015), and is still ongoing. This so-called Fukushima mapping project, which is a series of large-scale environmental monitoring efforts using diverse methods aiming to obtain information on a variety of contamination conditions, has been conducted. In the project, air dose rates and deposition densities of radionuclides were continuously monitored at fixed locations and mobile monitoring systems were also employed.

Among them, to obtain fundamental data on contamination conditions in reference places that meet certain basic requirements described in section 2 of this paper, the measurement of dose rates in air in terms of ambient dose equivalent rates (hereafter, air dose rates) and radionuclide deposition densities on the ground (hereafter, deposition densities) have been conducted in undisturbed flat fields, where the basic topographical features were similar, and disturbance by human activities or flooding was unlikely to occur. Air dose rates were measured using standard survey meters in all cases (Mikami et al., 2015a). While, for to determine deposition densities, a large number of soil samples were collected and analyzed in the laboratory during the first campaign, which began in June 2011 (Saito et al., 2015), while in-situ measurements with a portable germanium detector have been employed since the second campaign (Mikami et al., 2015b).

We reported the features of air dose rates and deposition densities in undisturbed fields until December 2012 in previous papers (Saito et al., 2015; Mikami et al., 2015a, 2015b). In this paper, new original data obtained from 2013 to 2016 have been added to the previously reported data and are discussed throughout. Several radionuclides released from the accident were detected in soil over a widespread area soon after the accident. However, based rough estimations, radiocesium was found to be far more important than other radionuclides from a long-term exposure perspective. Thereafter, the environmental monitoring in the mapping project was primarily focused on radiocesium, and gamma-radiation emitting radionuclides other than radiocesium have not been detected since 2013. As previously mentioned, extensive monitoring has been continued in the mapping projects, and new knowledge on the contamination conditions and their temporal changes have been accumulated. Generally speaking, the air dose rates within the 80 km zone drastically decreased in the five years immediately after the accident.

A trend of air dose rates in undisturbed fields after radionuclide deposition was extensively investigated after the Chernobyl accident (Golikov et al., 2002; Likhtarev et al., 2002). The temporal change in the air dose rate was evaluated on the basis of radiocesium depth profiles repeatedly observed in many locations utilizing dose conversion coefficients, and analyzed using a bi-exponential function in Russia (Golikov et al., 2002) and for Ukraine (Likhtarev et al., 2002). The analysis indicated that the time-dependent air dose rate can be expressed by a combination of the short ecological half-life on the order of a few years and the long ecological half-life on the order of several tens of years.

The purpose of this paper is to discuss the temporal changes in air dose rates and radiocesium deposition densities performed at fixed locations in undisturbed fields between 2011 and 2016 after the FDNPP accident. The data from 2011 to 2012 have already been published (Saito et al., 2015; Mikami et al., 2015a, 2015b); however, parts of these results were used in the present study to evaluate temporal changes in contamination. First, an outline of the large-scale monitoring effort repeatedly conducted over the entire five-year period is described. The time-dependent decreasing tendency of the air dose rate and that of deposition densities are presented based on monitoring results. Further, the contents of the decrease are discussed according to the statistical analysis of the monitoring data, and a comparison of the air dose rate trend with that from the Chernobyl accident is also discussed.

2. Materials and methods

2.1. Measurement area and locations

As previously mentioned, this study discusses the trend of contamination conditions between 2011 and 2016, and therefore, the information on the measurement locations from the 2011 and 2012 monitoring efforts are described even though those results have already been published (Saito et al., 2015; Mikami et al., 2015a, 2015b). The large-scale environmental measurements were repeatedly taken through all campaigns conducted in the 80 km zone surrounding the FDNPP site, while the targeted area was broadened to examine the contamination conditions over wider areas in number of these campaigns. The trend in the contamination within the 80 km is the primary focus of this paper.

In the first campaign of the Fukushima mapping project in 2011, deposition densities of the accidently released radioactive materials were measured by gamma spectrometry of soil samples collected at approximately 2200 locations within the 100 km zone surrounding the FDNPP and other areas in Fukushima Prefecture (Saito et al., 2015). Since 2012, in-situ measurement using portable germanium detectors has been employed at approximately 380 locations within the 80 km zone (Mikami et al., 2015b). With respect to these in-situ measurements, the 80 km zone was divided into 5 km square grids, and one appropriate location in each square-shaped area was selected, resulting in the total of approximately 380 measurement locations. Fig. 1(a) presents a map of the in-situ measurement locations within the 80 km zone.

Air dose rates have been measured using survey meters at approximately 6500 locations also within the 80 km zone. In the measurements, the 80 km zone was divided into areas of 1 km square grids, and one appropriate location in each area was selected, resulting in a total of approximately 6500 locations. Measurement locations in 1 km square grids were primarily selected from inhabitable areas. In some campaigns, the targeted area was enlarged, and the number of measurement locations were changed. Fig. 1(b) presents a map of the air dose rate measurement locations within the 80 km zone. The number of measurement locations and periods for the air dose rate and the deposition density are presented in Tables 1 and 2, respectively.

For both types of measurements, fields which had a width of at least 5×5 m were selected, and this was the minimal requirement in situations where an ideal location could not be found in the target area. The air dose rate originating from the source within a 5 m radius amounts to about a half of the air dose rate from an infinite source for radiocesium exponentially distributed in soil at a relaxation mass depth of 1.0 g/cm^2 (Malins et al., 2015). If an object such as a tree or a shed existed outside the 5 m radius, it may act as a shielding material or as a source. However, unless the object is very large or heavily contaminated, the effect should be limited considering the projected solid angle. Most of the measurements were actually performed in wider fields. At each location, it was checked that the air dose rate did not significantly vary within an area of 3×3 m to avoid measurements in a heterogeneously contaminated area.

In addition, fields which would not be expected to be disturbed by human activities or flooding for a long time were intentionally selected to investigate natural weathering effects. Nevertheless, in some locations, decontamination work was performed or the surface conditions were changed, such as land that was plowed, graveled, or smoothed. In such cases, the information was recorded, and the analysis was performed separately depending on the circumstances.

Accordingly, the locations were organized into three categories: (1) decontaminated locations, (2) artificially changed locations, and (3) non-decontaminated locations. The decontaminated locations are locations where decontamination work was clearly performed at or nearby the particular site according to information obtained about the site. The artificially changed locations are locations where it was judged

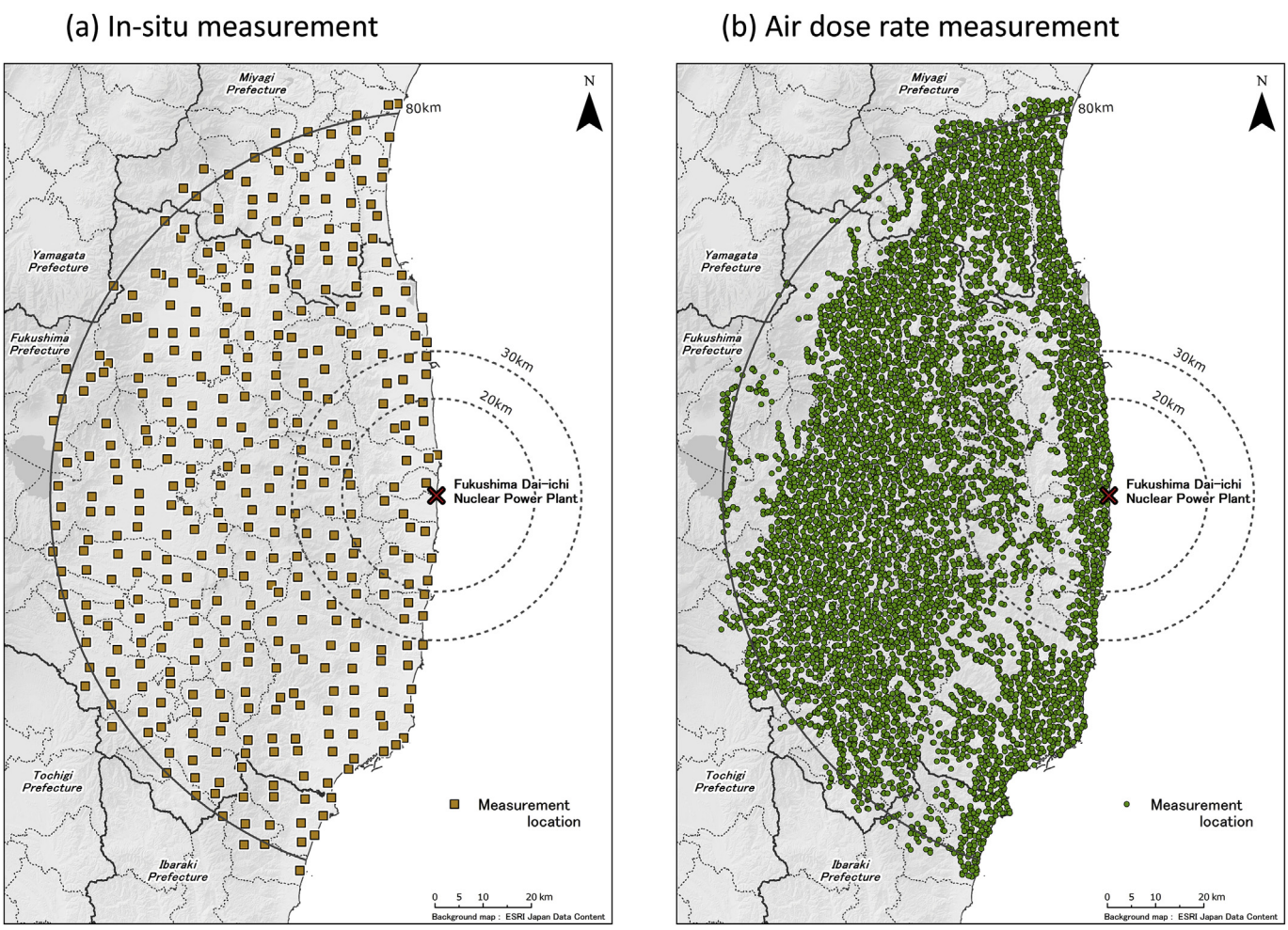

Fig. 1. Examples of locations for the in-situ measurements using portable germanium detectors and the air dose rate measurements using survey meters in September 2016.

based on the appearance or surface conditions that some artificial change to the ground was made such as plowing, ground leveling, and/or graveling. This case does not always indicate that decontamination work was performed; however, such artificial changes in most cases led to a decrease in air dose rates. Therefore, in statistical analysis, the artificially changed locations were included as part of the decontaminated locations, and their air dose rates were compared with those of the non-decontaminated locations, where no artificial activities including decontamination were performed. The term "undisturbed field" was originally intended to refer to a "non-decontaminated location". However, as a result, measurements were performed for a certain number of decontaminated or artificially changed locations as well. Thus, in this paper, we decided to use "undisturbed fields" as a general term to indicate measurement locations.

2.2. Measuring methods and procedures

In this section, methods and procedures are described for the measurement of radionuclide deposition and air dose rates conducted from 2013 to 2016.

2.2.1. Radionuclide deposition density

A portable germanium detector was taken out to an undisturbed field and placed on a tripod at a height of 1 m above the ground surface with the detector crystal facing downward. During the entire measurement campaign from 2011 to 2016, several different types of germanium detectors, which are cooled electrically or by liquid nitrogen having a relative efficiency of 10–40%, were used. Detailed information and regarding the germanium detectors used in this study and their comparative results are cited elsewhere (Mikami et al., 2018). A pulse-height spectrum was acquired, and the counts of a total-absorption peak for gamma rays emitted from the targeted radionuclide were converted to deposition density. The data acquisition time was set to 30 min since the 2013 campaigns because the short half-life nuclides had already decayed, and the time length was enough to obtain peak counts for determining radiocesium (^{134}Cs and ^{137}Cs) deposition densities within sufficiently low statistical uncertainties, which was less than a few percent. In some of the targeted locations from the second campaign of 2012, ^{110m}Ag was also detected, and after 2012, only radiocesium was observed.

Six or seven teams took part in the in-situ measurements at more than 380 locations in each campaign. At the beginning of each measurement campaign of a particular year, comparative analysis was conducted to ensure compatibility among the teams and measurement precision (Mikami et al., 2015c, 2018). Since 2012, the Japan Chemical Analysis Center (JCAC), Nuclear Safety Technology Center (NUSTEC), Institute of Radiation Measurements (IRM), and Japan Atomic Energy Agency (JAEA) has taken responsibility performing the measurements (Mikami et al., 2015b).

To evaluate the deposition density of a radionuclide and the air dose rate attributed to the radionuclide according to the EML method (Beck et al., 1972; Miller and Shebell, 1993), the relaxation mass depth β, which is a parameter indicating the degree of radionuclide penetration into the soil is necessary. When in-situ measurements began in each

Table 1
Number of measurement locations and periods for air dose rate maps.

Campaign	Measurement period (day/month/year)	Representation name of occasion	Targeted area	Number of measured locations	Frequency of measurement location
1[a]	4/6–8/7/2011	June 2011	Within a 100 km of the FDNPP and other areas in Fukushima Prefecture	2168	2 km × 2 km grids for the areas within an 80 km of the FDNPP and 10 km × 10 km grids for the areas beyond 80 km from the FDNPP
2[b]	13/12/2011–29/5/2012 except from January to March	March 2012	Region of Tohoku and Kanto	1016	5 km × 5 km grids for the areas with dose rate greater than 0.2μSv/h and 10 km × 10 km grids for where the air dose rate was less
3–1[b]	14/8–7/9/2012	August 2012	Within 80 km of the FDNPP	6551	1 km × 1 km grids
3–2[b]	5/11–7/12/2012	November 2012	Within 80 km of the FDNPP	6549	1 km × 1 km grids
4–1	3/6–4/7/2013	June 2013	Within 80 km of the FDNPP	6562	1 km × 1 km grids
4–2	28/10–4/12/2013	November 2013	Within 80 km of the FDNPP	6554	1 km × 1 km grids
5–1	15/7–5/9/2014	August 2014	Within 80 km of the FDNPP	6572	1 km × 1 km grids
5–2	4/11–5/12/2014	November 2014	Within 80 km of the FDNPP	6565	1 km × 1 km grids
6	3/8–8/9/2015	August 2015	Within 80 km of the FDNPP	6577	1 km × 1 km grids
7	22/8–4/10/2016	September 2016	Within 80 km of the FDNPP	6566	1 km × 1 km grids

[a] Saito et al. (2015).
[b] Mikami et al. (2015a).

measurement campaign, the most appropriate value of the β was not known. Therefore, evaluating the value from data obtained in previous campaigns was tentatively adopted. After obtaining measurements in each location, the deposition density was reevaluated using an appropriate β value determined from the depth profiles by soil sampling performed at approximately 85 locations in the 100-km radius area surrounding the FDNPP in the same campaign (Matsuda et al., 2015).

In addition to radiocesium, concentrations of natural radionuclides ^{40}K, ^{214}Bi, ^{214}Pb, ^{208}Tl, and ^{228}Ac in the soil were determined using in-situ spectrometry at 311 and 332 locations in 2014 and 2016, respectively. Bismuth-214 and ^{214}Pb were the dominant radionuclides in the ^{238}U decay series, and ^{208}Tl and ^{228}Ac were dominant in the ^{232}Th series. The concentrations of both radiocesium and natural radionuclides were converted to air kerma rates using the dose conversion coefficients tabulated in ICRU 53 (ICRU, 1994).

A comparison between the deposition densities obtained from in-situ spectrometry and soil sampling were conducted at eight locations in the first measurement campaign (MEXT, 2012). Five soil samples were collected within a 3 × 3 m square area at each location, analyzed at a laboratory, and the deposition density was calculated from the average concentration. In-situ spectrometry using a Ge detector was performed at the same location. The average ratio of radiocesium deposition density determined by soil sampling to that obtained by in-situ spectrometry was found to be 0.99 ± 0.24. For cases where the variation in radiocesium concentration among the five soil samples was relatively large, the discrepancy in deposition density between soil sampling and in-situ spectrometry were also large.

2.2.2. Air dose rate

The ambient dose equivalent rates were measured in principle at approximately 6500 locations in the 80 km zone in each campaign using NaI(Tl) scintillation survey meters (Hitachi TCS-171B or TCS-172B) and ionization-chamber type survey meters (Hitachi ICS-323C) depending on the magnitude of air dose rate being evaluated. The number of monitoring locations and targeted areas in each measurement campaign are presented in Table 1. When the air dose rates were more than 30 μSv/h, which is the upper limit of reliable measurements by the NaI(Tl) scintillation survey meters, ionization-chambers was used. Survey meters calibrated within the preceding 12 months before the measurements were used. The calibration was performed by makers or registered organizations using standard radiation sources or fields which were traceable to the national standards. The criteria for the selection of measurement locations, details of measurement conditions with the survey meter, and data recording procedures were the same as those reported in the literature (Mikami et al., 2015a). Air dose rates in terms of air kerma were also evaluated on the basis of results from in-situ spectrometry. They were used only to check the appropriateness of in-situ measurements, and not to create air dose rate maps.

2.3. Data analysis

2.3.1. Radionuclide deposition density

Deposition densities of ^{134}Cs and ^{137}Cs were evaluated from the peaks in the measured spectrum corresponding to the emitted gamma-ray energy of 605 keV and 662 keV, respectively, in accordance with ICRU Report 53 (ICRU, 1994). As dominant natural radionuclides, concentrations of ^{214}Pb, ^{214}Bi, ^{208}Tl, ^{228}Ac, and ^{40}K were evaluated using 352 keV, 1765 keV, 583 keV, 911 keV, and 1461 keV gamma rays, respectively.

As described in a previous study (Mikami et al., 2015b), the deposition density was calculated under the assumption that a gamma-ray spectrum was measured under ideal conditions, with the detector was located in an open and flat field with no attenuation of the gamma rays by objects existing on the ground, the radionuclides were exponentially distributed in the depth direction of the soil, and the same exponential distribution extended infinitely in the horizontal direction. The

Table 2
Number of measurement locations and periods for deposition density maps.

Campaign	Measurement period (day/month/year)	Reference date of decay correction (day/month/year)	Targeted area	Number ofmeasured locations	Frequency of measurement location	Deposition density analysis method
1[a]	4/6–8/7/2011	14/6/2011	Within a 100 km of the FDNPP and other areas in Fukushima Prefecture	2168	2 km × 2 km grids for the areas within an 80 km of the FDNPP and 10 km × 10 km grids for the areas more than 80 km from the FDNPP	Gamma spectrometry of sampled soils
2[b]	13/12/2011–29/5/2012 except from January to March	1/3/2012	Region of Tohoku and Kanto	1016	5 km × 5 km grids for the areas with dose rate greater than 0.2μSv/h and 10 km × 10 km grids for where the air dose rate was less	In situ gamma spectrometry
3–1[b]	13/8–19/9/2012	1/9/2012	Within 80 km of the FDNPP	381	5 km × 5 km grids	In situ gamma spectrometry
3–2[b]	5/11–12/12/2012	1/12/2012	Within 80 km of the FDNPP	380	5 km × 5 km grids	In situ gamma spectrometry
4–1	3/6–10/7/2013	1/7/2013	Within 80 km of the FDNPP	381	5 km × 5 km grids	In situ gamma spectrometry
4–2	28/10–6/12/2013	1/12/2013	Within 80 km of the FDNPP	381	5 km × 5 km grids	In situ gamma spectrometry
5–1	23/6–30/7/2014	1/7/2014	Within 80 km of the FDNPP and region of Tohoku and Kanto	437	5 km × 5 km grids	In situ gamma spectrometry
5–2	27/10–5/12/2014	1/12/2014	Within 80 km of the FDNPP and region of Tohoku and Kanto	437	5 km × 5 km grids	In situ gamma spectrometry
6	24/8–7/10/2015	1/10/2015	Within 80 km of the FDNPP	382	5 km × 5 km grids	In situ gamma spectrometry
7	24/8–6/10/2016	1/10/2016	Within 80 km of the FDNPP	383	5 km × 5 km grids	In situ gamma spectrometry

[a] Saito et al. (2015).
[b] Mikami et al. (2015b).

Table 3
Relaxation mass depth assumed in the evaluation of in situ spectrometry results.

Campaign	Middle day of a soil sampling campaign	Geometric mean of β value
	(day/month/year)	(g cm^{-2})
2	22/12/2011	1.13
3–1	28/8/2012	1.31
3–2	30/11/2012	1.51
4–1	9/6/2013	1.79
4–2	3/11/2013	2.14
5–1	18/7/2014	2.27
5–2	8/11/2014	2.36
6	10/9/2015	2.95
7	12/9/2016	3.13

relaxation mass depth β indicating the degree of radiocesium penetration into the soil in the exponential function was the essential parameter used in the evaluation of deposition density. At some measurement locations, this assumption was not sufficiently valid; for example, some locations were not ideally open or completely flat. The effect of variation in the ^{137}Cs depth profile on the evaluated deposition density was estimated to be a maximum of a few tens of percent (NRA, 2017).

At more than 80 locations over 80 km zone surrounding the FDNPP, depth profiles were investigated using layer-by-layer soil sampling with a scraper plate (Matsuda et al., 2015). In principle, soil up to a depth of 10 cm was collected at 0.5 cm intervals in the upper soil region and at one to a few cm intervals in deeper parts. At approximately 40% of locations where radiocesium depth profile was investigated, the highest radiocesium concentration was not observed at the ground surface but at a certain depth, and the depth profile was not well fitted by an exponential function. In these cases, an effective β value β_{eff} was determined so that the relationship between the air dose rate at 1 m above the ground and β_{eff} became the same as that for the exponential function (Matsuda et al., 2015). The average β values adopted for data processing in each campaign are presented in Table 3, which were calculated by averaging the all β values obtained for exponential distributions and the all β_{eff} values for non-exponential distributions (NRA, 2016).

The air kerma rates evaluated from spectra measured by portable germanium spectrometers and those measured by hand-held survey meters at the same time and same position were compared. Fig. 2 shows scatter plots between the air kerma rates evaluated by in-situ gamma spectrometry and those measured by survey meters in 2016. The air dose rates in terms of the air kerma rate (μGy/h) obtained using both methods displayed good agreement, and the slope of the regression line and their coefficient of determination were both nearly 1. This indicated that the measurements were appropriately performed with sufficient statistical accuracy. In these ways, the reliability of the estimated deposition densities was confirmed during every measurement campaign, and these deposition densities were plotted on a map with the Global Positioning System (GPS) data.

2.3.2. Air dose rate

Distribution maps of the air dose rates at 1 m above the ground from ten different occasions over the five-year period (2011–2016) were created from the obtained dose rate data and positional data. Correction of the measured air dose rate based on the half-lifes of the radionuclides during each measurement campaign was not implemented because the radioactive decay in the period was sufficiently smaller than the measurement uncertainty of the survey meter (~15%), as described in a previous study (Mikami et al., 2015a). The temporal change in the air dose rates was examined by comparing the air dose rates obtained at the same locations between 2011 and 2016.

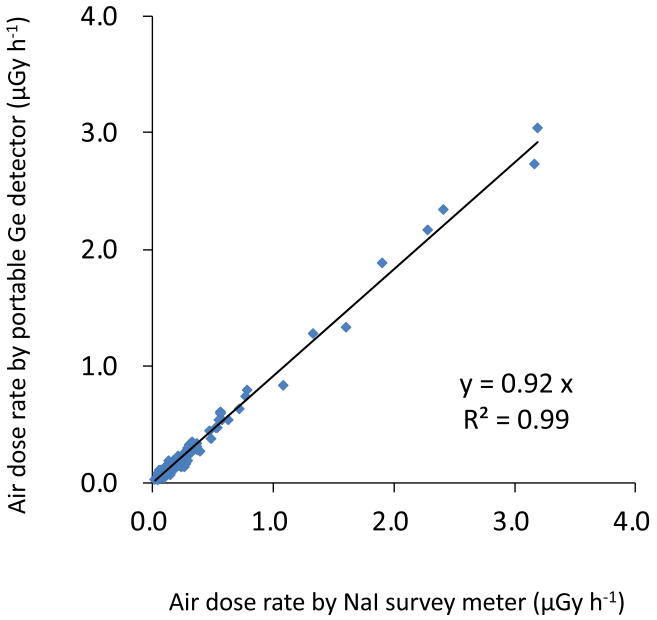

Fig. 2. Scatter plot of the air dose rate in terms of air kerma measured by NaI (Tl) scintillation survey meters and by portable germanium detector. The line is a simple liner regression line with no intercept. R^2 value represents coefficient of determination.

2.3.3. Refinement of a radiocesium deposition map utilizing the correlation between air dose rate and deposition density

Deposition densities of ^{134}Cs and ^{137}Cs were well correlated with the air dose rate in any campaign. This is because radiocesium has been a dominant contributor to the air dose rate since the first campaign (Saito et al., 2015) and the variation in the β value did not significantly affect the air dose rate. Scatter plots of the air dose rates and deposition densities of ^{134}Cs or ^{137}Cs measured at same position in 2016 are shown in Fig. 3 as an example. Using such good correlativity, refined deposition density maps were created from air dose rates measured at approximately 6500 locations in every campaign for the five-year period.

3. Results and discussions

3.1. Distribution of air dose rates and radiocesium deposition densities

The maps created for air dose rates and deposition densities of ^{134}Cs and ^{137}Cs from 2011 to 2016 are provided in the supporting data (Figs. S1–S3, respectively). For ^{134}Cs and ^{137}Cs, the refined maps described in the previous section are demonstrated in Figs. S2 and S3. As seen in Fig. S1, the air dose rates in the 80 km zone have prominently decreased with elapsed time since June 2011. The essential cause of the air dose rate decrease over this five-year period clearly appeared to be the radioactive decay of ^{134}Cs with a half-life of 2.06 y. The deposition densities of ^{134}Cs have drastically decreased with time as shown in Fig. S2; on the contrary, the reduction on the ^{137}Cs in Fig. S3 was not particularly significant over the five years. Since the contribution of ^{134}Cs to the air dose per unit of deposition density is 2.7 times greater than that of ^{137}Cs (Saito and Petoussi-Henss, 2014), the radioactive decay of ^{134}Cs has greatly contributed to the decrease in air dose rates in the 80 km zone during the initial five years. Further, the penetration of radiocesium into the soil and decontamination work were considered to have contributed to the air dose rate decrease. This is discussed in the next section.

The relative frequency distributions of the air dose rates within the 80 km zone are illustrated in Fig. 4. Data from campaign 2 (see Table 1) is not plotted in Fig. 4 because of the small number of data due to the measurement grids, which were larger than other campaigns. The

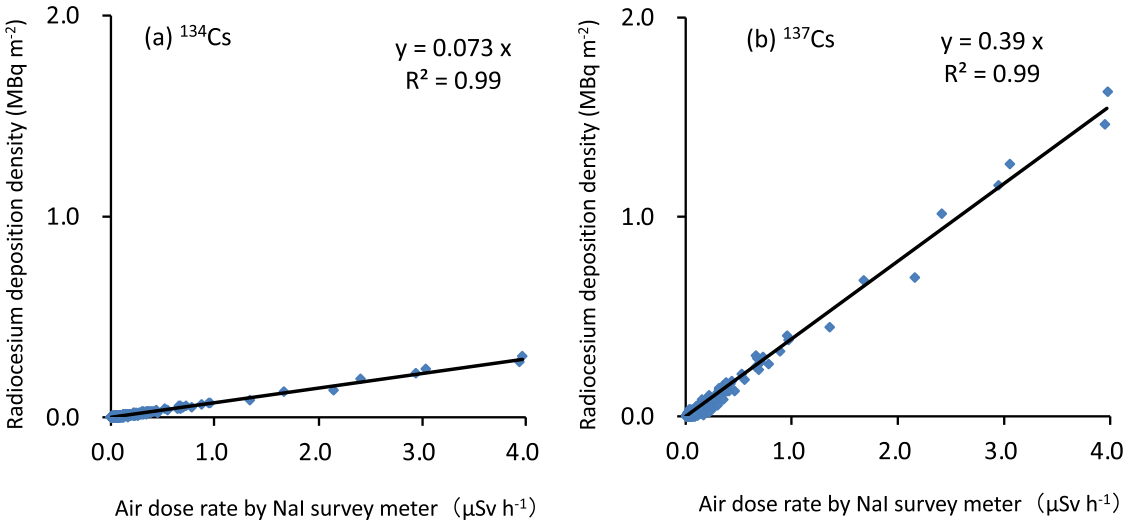

Fig. 3. Scatter plot of the air dose rate in terms of air kerma measured by NaI(Tl) scintillation survey meters and radiocesium deposition density evaluated by in-situ spectrometry. The lines are simple liner regression lines with no intercept. R^2 value represents coefficient of determination. (Left:^{134}Cs, Right:^{137}Cs).

locations with air dose rates more than 0.2 μSv/h have steadily decreased, whereas the areas less than 0.2 μSv/h have increased. The proportion of the locations less than 0.2 μSv/h in the 80 km zone was 15% in 2011, while it was 75% in 2016. The proportion was 53% in 2011 and 93% in 2016 based on data from locations that was less than 0.5 μSv/h. Fig. 5 gives the relative frequency distributions in the evacuation areas issued on September 5, 2015 according to the latest digital data of the area boundary that was obtained. Results from the second campaign were not plotted due to the same reason associated with Fig. 4. In principle, the evacuation areas were determined according air dose rates that exceeded 3.8 μSv/h, which is supposed to roughly correspond to an annual exposure dose of 20 mSv to the inhabitants. This supposition was determined for external exposure based on quite simple assumptions related to life patterns, dose reduction effect by houses, and other factors, which resulted in a substantial overestimation of doses. The areas with air dose rates smaller than 3.8 μSv/h were actually contained to a certain degree within the evacuation area, even in June 2011 because the criteria was not rigorously adopted based on data measured on the ground. The frequency in the air dose rate was highest in the dose rate range of 3.8–9.5 μSv/h up until November 2012, after which it shifted to lower dose rates. In September 2016, the air dose rate frequency was highest in the range of 0.2–0.5 μSv/h, and the air dose rates have decreased significantly over the entire 80 km zone, including the evacuation area.

3.2. Ratio of air dose rates between 2011 and 2016

In Fig. 6, the air dose rates observed in September 2016 were compared with those in June 2011 (Mikami et al., 2015a). In the case of the positional data collected by GPS agreed within a distance of 20 m between 2011 and 2016, it was assumed that the measurements were made at the same position since the positional resolution of the GPS was approximately 20 m, and the comparison was made. The air dose rate varied significantly depending on the location, even within a range of 20 m and especially in highly contaminated areas due to the horizontal variability of deposited radiocesium. Thus, the precision of 20 m may cause a non-negligible fluctuation in the air dose rate measured at the same position based on GPS data. Hereafter, whenever temporal change

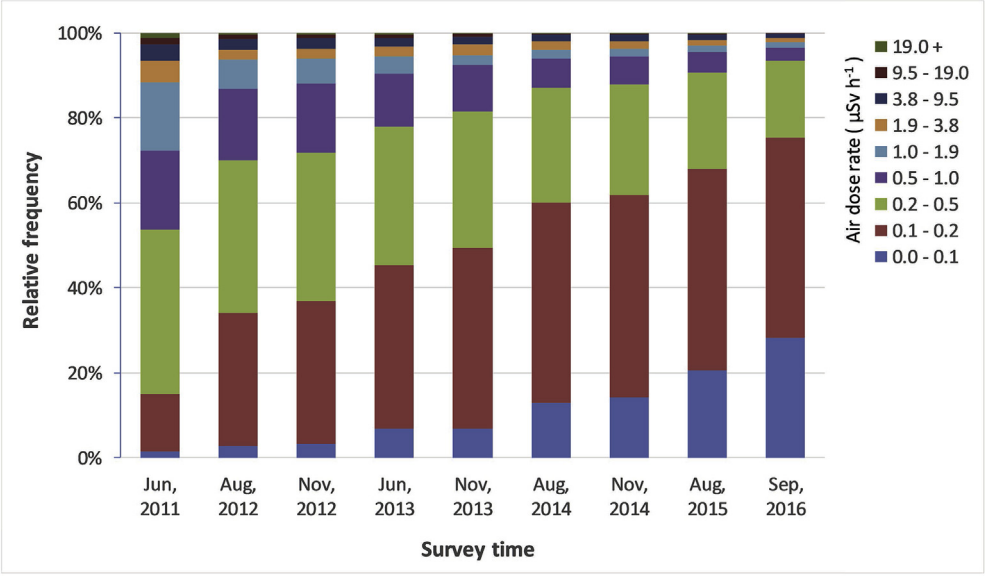

Fig. 4. Relative frequencies of air dose rates in 80 km zone from FDNPP for nine different time periods. The new original data obtained in 2013–2016 were added to the previously reported data (Mikami et al., 2015a).

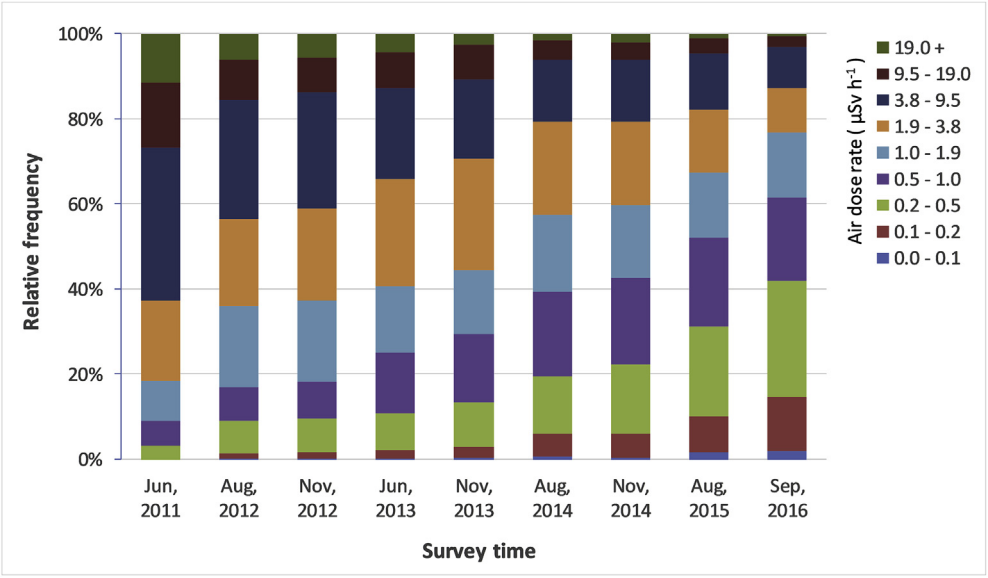

Fig. 5. Relative frequencies of air dose rates in evacuation area as of September 2015 for nine different time periods.

is discussed, the contribution of natural gamma rays to the air dose rates was subtracted from the observed air dose rates assuming that a contribution of 0.05 μSv/h (Fukushima prefecture, 2010) does not change depending on the location. The air dose rate due to natural radionuclides did in fact change according to the location. We obtained some data on location-dependent natural radionuclide concentrations and air dose rates, which are described later. These data did not contain the all natural radionuclides. In addition, the effect of air dose rate variation was not significant. Therefore, a constant air dose rate of 0.05 μSv/h originating from natural radionuclides was assumed.

Fig. 6(a) demonstrates the comparison for the entire air dose rate range, and Fig. 6(b) for the range whose initial air dose rates were less than 5 μSv/h, where a great portion of data exists. The slopes of the regression lines for the entire air dose rate range were 0.13 ± 0.01 and 0.23 ± 0.004 for the decontaminated and non-decontaminated locations shown by red triangles and blue circles, respectively. As a whole, the decontaminated locations clearly displayed a faster reduction of the dose rate compared to that of the non-decontaminated locations. The slope of the regression line for all locations was 0.19 ± 0.004. When the air dose rate range was limited to less than 5 μSv/h, the slopes of the regression lines as for the decontaminated, non-decontaminated, and all locations were 0.095 ± 0.004, 0.19 ± 0.003, and 0.14 ± 0.003 respectively. These values were smaller than those associated with the entire air dose rate range: the air dose rate reduction was faster for locations displaying values less than 5 μSv/h. This is likely due to the fact that decontamination was actively performed in areas with air dose rates less than 3.8 μSv/h, and the areas were affected by decontamination even if the measurement location was not directly decontaminated because gamma rays coming from a distance were depressed.

The numerical data of the comparison are shown in Table 4. The ratio of the summation of air dose rate in 2016 to that in 2011 was calculated as an indicator of air dose rate change in addition to the slope of the regression line. The average air dose rate was obtained if the summation was divided by the number of locations, and thus, the comparison of the summation substantially refers to the comparison of the average. Since the ratio of the summation cannot give the

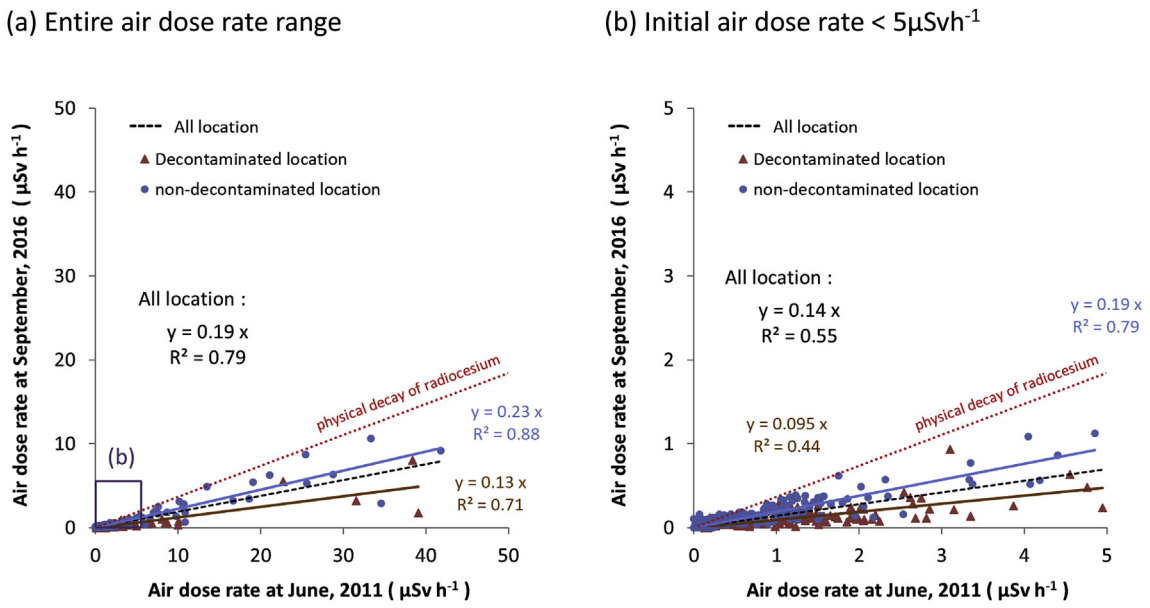

Fig. 6. Scatter plots of the air dose rate measured in 2011 and 2016. Physical decay of radiocesium is shown as red dotted lines.

Table 4
Ratios of air dose rate in 2016 normalized to that in 2011.

	Ratio of summation[a]	Averaged ratios[b]	Slope of regression line[c]
All location	0.18	0.21 ± 0.12	0.19 ± 0.004
Decontaminated location [d]	0.11	0.13 ± 0.09	0.13 ± 0.01
Non-decontaminated location	0.23	0.25 ± 0.11	0.23 ± 0.004

As a comparison, the expected ratio from radioactive decay of radiocesium is 0.37.
[a] Ratio of summation of air dose rates (2016/2011).
[b] Averaged value of ratios of air dose rates (2016/2011) in each location. Errors are standard deviations.
[c] Slope of regression line obtained from Fig. 6 (a). Errors are standard errors.
[d] Artificially changed locations are included.

information of data variance, the mean of the air dose ratio in each location (referred to as the "averaged ratio") was also calculated. To avoid fluctuation of the ratio in a low air dose rate range, where the air dose rate due to radiocesium was comparable to the background radiation level, the locations with air dose rates greater than 0.1 μSv/h in the first campaign were used for the calculation.

As shown in Table 4, the ratio of the summation of air dose rates between 2011 and 2016 was 0.18, 0.11, and 0.23 for all locations, the decontaminated locations, and non-decontaminated locations, respectively. The averaged ratio of air dose rates in each location was 0.21, 0.13, and 0.25, respectively. The three different quantities indicating the attenuation of air dose rates from 2011 till 2016, that is the ratio of the summed air dose rate, the averaged ratio of air dose rates and the slope of the regression lines, provided similar values in all cases. The air dose rate due to deposited radiocesium in the fields was found to have decreased to about 20% of the initial value on average. The air dose rate was estimated to be 0.37 according to radioactive decay during this period. Therefore, the air dose rate decreased to about a half of that expected from physical decay between 2011 and 2016.

When decontaminated and non-decontaminated locations were compared, the air dose rates in decontaminated locations were approximately one half of those in non-decontaminated locations. In addition, statistical tests (Mann-Whitney *U* test) showed a significant difference ($p < 0.01$) for the averaged ratios between non-decontaminated locations and decontaminated locations. A comparison of air dose rates between all locations and the non-decontaminated locations in Table 4 suggests that decontamination and other human activities that changed ground conditions had reduced the average air dose rate by up to 20%, even though the representation of the absolute value must be carefully checked in the future.

The air dose rates in non-decontaminated locations decreased faster than radioactive decay. This reduction can be largely explained by the penetration of radiocesium into the soil. The effective relaxation mass depth β was estimated to be 1.1 g/cm^2 in December 2011 and 3.1 g/cm^2 in September 2016; and this change corresponded to a decrease in the air dose rate to approximately 0.73. This value is close to the excess reduction rate observed in non-decontaminated locations (0.23/0.37 = 0.62). Thus, it is likely that the excess dose rate reduction in undisturbed fields was largely due to the penetration of radiocesium into the soil. Though, it is anticipated that some decontaminated locations could be included in the statistics of non-decontaminated locations even if decontamination was actually conducted due to the lack of available information.

3.3. Temporal change of deposition densities and air dose rate

The time-dependent tendency of the air dose rates relative to the first campaign (June 2011) in the 80 km zone is shown in Fig. 7; (a) averaged ratios and (b) ratios of summation of air dose rates, together with the air dose rate reduction expected due to radioactive decay of radiocesium. The dose rate reduction curve considering both the radioactive decay and the increase in shielding effect by vertical penetration of radiocesium into the ground is also shown. The data are separately shown for the all locations and the non-decontaminated locations. The ratios for all locations were always smaller than that for non-decontaminated locations, and the difference has been enhanced with elapsed time. Statistical tests (Mann-Whitney *U* test) showed a significant difference ($p < 0.01$) between decontaminated locations and non-decontaminated locations after the 3rd campaign (campaign 3–1, 2012, approximately 530 days after the accident). The difference between all locations and non-decontaminated locations after the 3rd campaign in Fig. 7 is attributed to the statistically significant difference between decontaminated locations and non-decontaminated locations. The 3rd campaign corresponded to the initiation of active decontamination work conducted in restricted areas. This suggests that the progress of decontamination work has contributed to a decrease in air dose rates, though the absolute effect of decontamination must be carefully considered since it is not known for certain how the measurement locations represent entire areas. It is important to note that all of the decontaminated locations out of approximately 6500 locations could not be identified, so a considerable number of decontaminated locations may be included in non-decontaminated datasets in the statistical analysis. For this reason, there may be a difference between plots for non-decontaminated location and a line for physical decay modified with the change in relaxation depth in Fig. 7. Further analysis of the data based on certain information on decontamination for all locations would be valuable to better understand this aspect.

The decreasing tendency of the average deposition density measured by in-situ gamma spectrometry was demonstrated in Fig. 8 both for ^{134}Cs and ^{137}Cs with the radioactive decay. The whole data were normalized to the average ^{137}Cs deposition density in March 2012, when in-situ gamma spectrometry began. Fig. 8(a) indicates the data for all locations within the 80 km zone, and Fig. 8(b) presents the data for non-decontaminated locations. For both isotopes of radiocesium, the average deposition density in non-decontaminated locations decreased almost in accordance with radioactive decay, which indicated that the horizontal movement of radiocesium is relatively small in undisturbed fields. This finding agrees with the results from a radiocesium migration study using test plots in Fukushima (Yoshimura et al., 2015). If we check in detail, the relative average deposition density of ^{137}Cs estimated by physical decay is 0.90, that of ^{134}Cs is 0.16 in 2016 (approximately 2030 days after the accident), while the observed average deposition density of ^{137}Cs was 0.82, that of ^{134}Cs was 0.15. Hence, the average deposition density in 2016 was lower than that expected from radioactive decay by approximately 10% both for ^{134}Cs and ^{137}Cs. Apart from shielding effect from vertical migration down in the soil, the explanation for this excess reduction may be due to the inclusion of decontaminated locations in the data for non-decontaminated locations.

The difference between Fig. 8(a) and (b) demonstrates the reduction in deposition density by decontamination; however, the discussion on the effect of decontamination is difficult because the deposition densities determined in the decontaminated locations include some degree of error due to usage of inappropriate β values. The large uncertainties associated with the determination of deposition density were influenced by horizontal variability, especially on the borders between

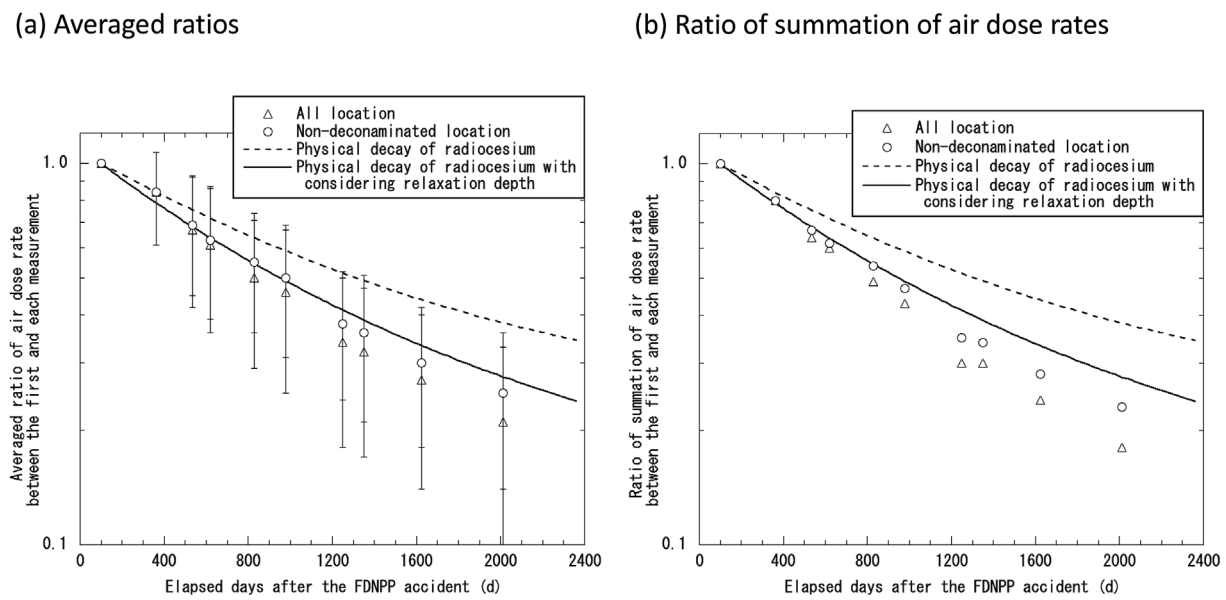

Fig. 7. Time-dependent tendency of air dose rates relative to the first campaign (June 2011) in 80 km zone from FDNPP. Dotted lines represent reduction curves due to radiocesium decay, and solid ones represent those expected under consideration of both radiocesium decay and change of relaxation mass depth.

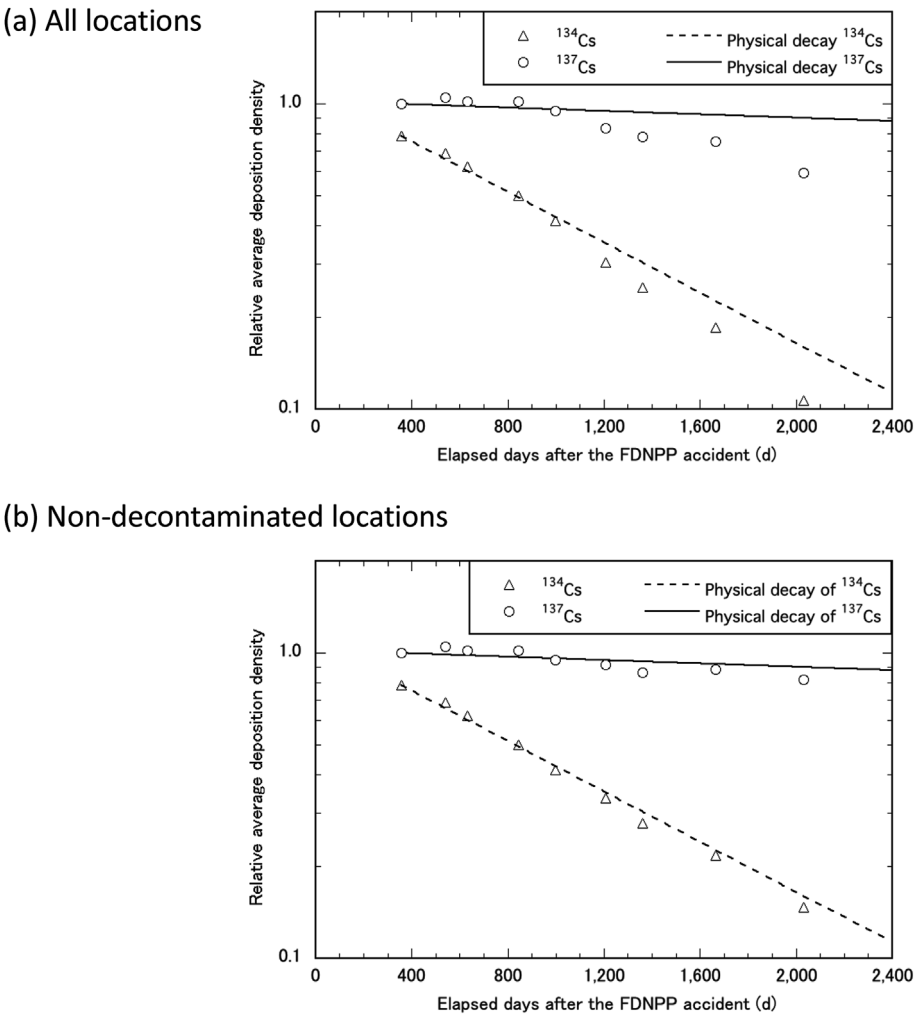

Fig. 8. Time-dependent tendency of average deposition density. Triangles and circles are relative deposition density for ^{134}Cs and ^{137}Cs, respectively. Blue and red lines represent physical decay curves of ^{134}Cs and ^{137}Cs, respectively.

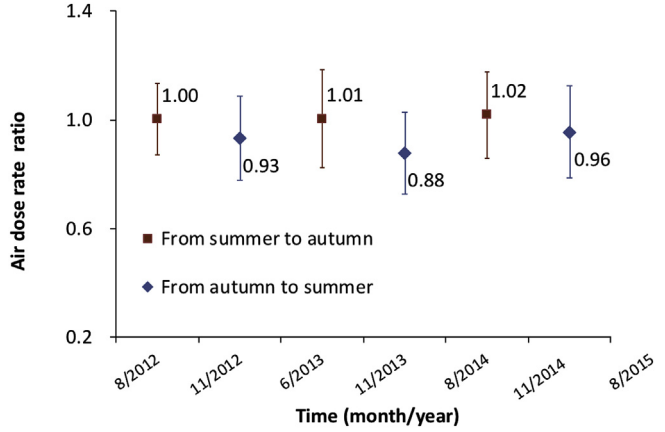

Fig. 9. Relative air dose rates between two measurement campaigns in non-decontaminated locations from 2012 to 2015. The relative dose rates excluding physical decay are given for two periods: from summer to autumn (red squares) and from autumn to summer (blue diamonds). (For interpretation of the references to colour in this figure legend, the reader is referred to the Web version of this article.)

decontaminated and non-decontaminated surfaces. Further investigation is necessary to obtain a realistic evaluation of deposition density in decontaminated fields.

3.4. Seasonal variation in air dose rate reduction

The reduction rate of air dose rates in undisturbed fields was found to change depending on the season in a year. To clarify the seasonal variation, we selected the air dose rate data obtained from 2012 till 2015, because the measurements were performed two times per year at similar occasions. Fig. 9 shows the ratio of the decay-corrected average air dose rates at the non-decontaminated locations between the two closest measurement campaigns. The first campaign in a year was performed in summer (August or June) and the second in autumn (November). Therefore, the decay-corrected ratio between the first and the second campaigns in a year indicates the air dose reduction due to ecological causes from summer to autumn; the ratio between the second campaign and the first campaign of the next year indicates the reduction from autumn to summer, though the length of the periods is not same. The dose rate reduction appeared to take place mainly from autumn to summer, but not as clearly from summer to autumn. The changes in decay-corrected average dose rate ratios from autumn to summer were found to be statistically different from those summer to autumn ($p < 0.05$, *t*-test). This indicates that there is a difference that cannot be explained by the length of the periods in the reduction rate of air dose rates.

Based on successive measurements, a previously conducted study suggested that the reduction of air dose rates was exclusively large within a few months from May (Yoshida et al., 2015), which coincides with the present observation. A correlation of the reduction with precipitation was not observed; therefore, the migration of radiocesium due to flooding or the variation in water content in soil could not be considered to be the direct causes of the change. The water content in soil is an important factor related to changes in the air dose rate in the environment; increasing water content tended to decrease the air dose rate due to increasing shielding effect against gamma rays. However, it has not been reported that water content in soil is significantly more in August or June. The reasons for the biased dose rate reduction tendency were not very clear, but bioturbation may be one of the reasons since activity of ambient biota very frequently occurs in the corresponding season. The change in depth profiles due to bioturbation has been investigated for a long time. Specifically, it has been reported that activity of earthworm has non-negligible influence on the transport of nuclides in soil (Bunz, 2002; Resner et al., 2011). This is just one possibility, and further study is necessary to determine the true reason for the seasonal bias tendency.

3.5. Air dose rates from natural radionuclides

Air dose rates from natural radionuclides distributed on the ground were evaluated using in-situ spectrometry by portable germanium detectors in 2014 and 2016. The average concentrations of ^{40}K, ^{214}Bi, ^{214}Pb, ^{208}Tl, and ^{228}Ac in the surface soil were converted to air kerma rates using dose conversion factors in ICRU 53 (ICRU, 1994). Bismuth-214 and ^{214}Pb were the dominant radionuclides among the ^{238}U series, and their contribution to the air dose rate was estimated to be 98% of that from all radionuclides in the decay series (Saito and Jacob, 1998). In addition, the contribution of ^{208}Tl and ^{228}Ac, which were the dominant radionuclides among the ^{232}Th series, was estimated to be 90% of that from all radionuclides in the series. The average air kerma rates from these all natural radionuclides determined in 2014 and 2016 were 0.039 ± 0.015 and 0.033 ± 0.012 μGy/h, respectively. These corresponded to 0.047 ± 0.018 and 0.039 ± 0.014 μSv/h, respectively, in terms of ambient dose equivalent rate, taking into account the fact that the ratio of ambient equivalent dose to air kerma was 1.2 for natural gamma rays (Saito and Endo, 2014). The background dose rate of 0.05 μSv/h assumed in section 3.2 was confirmed to be appropriate if all natural radionuclides that were not covered in the above analysis were taken into account.

3.6. Comparison of air dose rate decrease with that after the chernobyl accident

To express the air dose rate decrease due to penetration of radiocesium into the ground after the Chernobyl accident, the following bi-exponential equation was employed (Golikov et al., 2002; Likhtarev et al., 2002);

$$r(t) = p_1 \exp(-\ln 2\ t\ /T_1) + p_2 \exp(-\ln 2\ t\ /T_2)$$

Where $r(t)$ is the attenuation function expressing the relative air dose rate at time t after the deposition in undisturbed fields; T_1 and T_2 are the ecological half-lives of the fast attenuation component and the slow attenuation component, respectively; p_1 and p_2 are parameters showing the degree of the contributions from the fast and slow components. This attenuation function was intended to express the decrease in air dose rates due to penetration of radiocesium into the ground, and the effect of radioactive decay was excluded. For this purpose, the attenuation tendencies of air dose rates after the Chernobyl accident were evaluated based on the change in the observed depth profile of radiocesium in soil using dose conversion coefficients on the assumption that radiocesium does not decay with the physical half-lives. Then, the evaluated attenuation tendency was fitted to the bi-exponential function. The parameter values determined by Golikov et al. (2002) for Russian territories were $p_1 = 0.57$, $p_2 = 0.58$, $T_1 = 2.4$ y, and $T_2 = 37$ y; those by Likhtarev et al. (2002) for Ukrainian territories were $p_1 = 0.46$, $p_2 = 0.69$, $T_1 = 1.5$ y, and $T_2 = 50$ y. In their studies, the attenuation factor was normalized to the air dose rate for a plane source at a depth of 0.5 g/cm^2 with the same deposition density; therefore, the summation of p_1 and p_2 exceeds 1.0.

The attenuation of air dose rate calculated using the formula and the determined parameters during the same duration to our observation, that is about five years after the deposition, was estimated to be 0.58 for Russia and 0.62 for Ukraine. The attenuation of air dose rate, evaluated in a similar manner according to depth profile observed after the Fukushima accident, was 0.73 as mentioned above. This suggests that the penetration of radiocesium into soil in Fukushima has been slightly slower than those reported after the Chernobyl accident; it may reflect stronger fixation of radiocesium to soil particles in Fukushima

(Okumura et al., 2018). While, the actual observed average attenuation of air dose rates in non-decontaminated locations in this study was calculated to be 0.62 after decay correction. The cause of the discrepancy between 0.73 and 0.62 is possible due to the fact that some of the non-decontaminated locations were actually decontaminated but not recognized or affected by decontamination performed in surrounding areas as discussed previously. While the average attenuation of air dose rates for all locations was 0.49, which is obviously smaller than those described above. This suggests that human activities including decontamination significantly contributed to the decrease in air dose rates in the reference measurements locations.

4. Conclusions

Air dose rates and radionuclide deposition densities over the entire 80 km zone surrounding the FDNPP were measured in undisturbed fields from 2011 to 2016 at a frequency of once or twice a year to investigate the temporal change of the contamination conditions in reference locations. The detailed maps on air dose rates and deposition densities for ^{134}Cs and ^{137}Cs were constructed on the measurement data. The air dose rates drastically decreased in the five years immediately after the accident, and the average air dose rate in September 2016, excluding the background contribution, became about 20% of that in June 2011. The essential cause of the decrease was the physical decay of ^{134}Cs with a half-life of 2.06 y. The contribution to the air dose rate reduction over the same period from the physical decay of ^{137}Cs with a half-life of 30.2 y was limited. The average deposition densities of radiocesium in non-decontaminated fields were found to have decreased almost according to physical decay both for ^{134}Cs and ^{137}Cs, suggesting that the horizontal movement of radiocesium was relatively small as a whole. The air dose rates in undisturbed fields decreased eminently faster than expected from radioactive decay, and this was most likely due to the penetration of radiocesium into the soil resulting in the increase of shielding effects for gamma rays emitted from radiocesium in not on the soil surface. Results of this study further indicated that the decontamination work extensively conducted after the accident effectively decreased the air dose rate because the reduction in contamination conditions was observed in terms of both air dose rates and deposition densities. The reduction in air dose rates in non-decontaminated locations was found to occur mostly in the early summer, though the cause is not very clear. The decreasing tendency of air dose rates due to radionuclide penetration in soil was slower than those reported after the Chernobyl accident, whereas the actual observed decreasing trend in undisturbed flat fields in Fukushima was faster than those anticipated from the penetration effects.

Acknowledgment

This study was conducted as a part of the mapping projects funded by the Ministry of Education, Culture, Sports, Science and Technology (MEXT) and the NRA, Japan. The authors would like to express our sincere appreciation to all the people who directly and indirectly supported these Fukushima mapping projects. In particular, we would like to thank Prof. T. Nakamura and Momoshima and all the members of the ad hoc committee. We would also like to thank Dr. Rodolfo Gurriaran, Dr. Stéphanie Demongeot of IRSN, Dr. Fumiaki Takahashi of JAEA, Dr. Hiroaki Kato of Tsukuba University, and Dr. Takashi Saito and Dr. Mamoru Fujiwara of Osaka University for their technical support and cooperation in the Fukushima mapping project in 2011, as they were still struggling against a shortage of ready-to-dispatch specialists and instrumentation in the aftermath of the Fukushima accident. We are also grateful to Mr. Masanao Nakano of IDC and Mr. Daisuke Ishikawa of JREC for their support on technical and administrative task for the measurement campaigns. We also thank Mr. Kiichiro Uno and Mr. Yoshimi Urabe of NESI for his dedicated assistance for data analysis and mapping.

Appendix A. Supplementary data

Supplementary data to this article can be found online at https://doi.org/10.1016/j.jenvrad.2019.03.017.

References

Beck, H.L., et al., 1972. In Situ Ge(Li) and NaI(Tl) Gamma-Ray Spectrometry. HASL-258.
Bunz, l. K., 2002. Transport of fallout radiocesium in the soil by bioturbation: a random walk model and application to a forest soil with a high abundance of earthworms. Sci. Total Environ. 293, 191–200.
Fukushima prefecture, TEPCO, 2010. FY2010 Nuclear Power Plant Environmental Radioactivity Measurement Report. (in Japanese).
Golikov, V. Yu, et al., 2002. External exposure of the population living in areas of Russia contaminated due to the Chernobyl accident. Radiat. Environ. Biophys. 41, 185–193.
IAEA, 2015. The Fukushima Daiichi Accident. 978-92-0-107015-9.
ICRU, 1994. Gamma-ray spectrometry in the environment. ICRU 53.
Katata, G., et al., 2015. Detailed source term estimation of the atmospheric release for the Fukushima Daiichi Nuclear Power Station accident by coupling simulation of an atmospheric dispersion model with an improved deposition scheme and oceanic dispersion model. Atmos. Chem. Phys. 15, 1029–1070.
Likhtarev, I., et al., 2002. Chernobyl accident: retrospective and prospective estimates of external dose of the population of Ukraine. Health Phys. 82, 290–303.
Matsuda, N., et al., 2015. Depth profiles of radioactive cesium in soil using a scraper plate over a wide area surrounding the Fukushima Dai-ichi Nuclear Power Plant, Japan. J. Environ. Radioact. 139, 427–434.
NRA, 2016. Investigation on depth profile of radiocesium in soil. Report on data aggregation project of radioactive materials distribution data associated with Fukushima Dai-ichi Nuclear Power Station Accident. https://radioactivity.nsr.go.jp/ja/contents/14000/13159/view.html, Accessed date: 20 March 2019 (in Japanese).
Malins, A., et al., 2015. Field of view for environmental radioactivity. In: Proceedings of the 2015 International Symposium on Radiological Issues for Fukushima's Revitalized Future. Paruse Iizaka, Fukushima City, Japan May 30-31.
MEXT, 2012. Report on Construction of Maps Indicating Air Dose Rate Distribution Etc. accessed 9.10.2018. http://radioactivity.nsr.go.jp/ja/contents/6000/5235/24/5253_20120615_1_rev20130701.pdf (in Japanese).
Mikami, S., et al., 2015a. The air dose rate around the Fukushima Dai-ichi Nuclear Power Plant: its spatial characteristics and temporal changes until December 2012. J. Environ. Radioact. 139, 250–259 2015.
Mikami, S., et al., 2015b. Spatial distributions of radionuclides deposited onto ground soil around the Fukushima Dai-ichi Nuclear Power Plant and their temporal change until December 2012. J. Environ. Radioact. 139, 320–343.
Mikami, S., et al., 2015c. *In situ* gamma spectrometry intercomparison in Fukushima, Japan. Jpn. J. Health Phys. 50, 182–188.
Mikami, S., et al., 2018. Guidance for *in situ* gamma spectrometry intercomparison based on the information obtained through five intercomparisons during the Fukushima mapping project. Under submission.
Miller, K.M., Shebell, P., 1993. In-situ Gamma-Ray Spectrometry. A tutorial for environmental radiation scientist EML-557.
NISA, 2011. Nuclear Industry Safety Agency). accessed 30.01.2014. http://www.meti.go.jp/press/2011/10/20111020001/20111020001.pdf (in Japanese).
NRA, 2017. In situ measurement method using a Germanium semi-conductor detector. Radiation Measurement Method Series 33. http://www.kankyo-hoshano.go.jp/series/main_pdf_series_33.html (in Japanese).
Okumura, M., et al., 2018. Radiocesium interaction with clay minerals: Theory and simulation advances Post-Fukushima. J. Environ. Radioact 189, 135–145.
Resner, K., et al., 2011. Elemental and mineralogical changes in soils due to bioturbation along an earthworm invasion chronosequence in Northern Minnesota. Appl. Geochem. 26, 5127–5131.
Saito, K., Jacob, P., 1998. Fundamental data on environmental gamma-ray fields in the air due to sources in the ground. JAERI-Data/Code 98–001.
Saito, K., Petoussi-Henss, N., 2014. Ambient dose equivalent conversion coefficients for radionuclides exponentially distributed in the ground. J. Nucl. Sci. Technol. 51, 1274–1287.
Saito, K., Endo, A., 2014. Measurement and evaluations of air dose rates around Fukushima III characteristics of environmental gamma rays and the exposure doses. Radioisotopes 63, 585–602 (in Japanese).
Saito, K., Onda, Y., 2015. Outline of the national mapping projects implemented after the Fukushima accident. J. Environ. Radioact. 139, 240–249.
Saito, K., et al., 2015. Detailed deposition density maps constructed by large-scale soil sampling for gamma-ray emitting radioactive nuclides from the Fukushima Daiichi Nuclear Power Plant accident. J. Environ. Radioact. 139, 308–319.
Yoshimura, K., et al., 2015. Evaluation of radiocesium wash-off by soil erosion from various land use using USLE plots. J. Environ. Radioact. 139, 362–369.
Yoshida, H., et al., 2015. Seasonal Change in the Reduction of the Air Dose Rate Observed by Daily Measurements. 2015 Fall Meeting. Atomic Energy Society of Japan (in Japanese).